Investigation of Headed Bar Joints between Precast Concrete Panels

Jean Paul Vella[a], Robert L. Vollum[a], Andrew Jackson[b]

[a]Department of Civil and Environmental Engineering, Imperial College London, UK

[b]Engineering Excellence Group, Laing O'Rourke, UK

Abstract

The paper addresses the design and behaviour of narrow cast in-situ joints between precast concrete elements in which continuity of reinforcement is achieved through overlapping headed bars. Using headed bars minimises the lap length required within the cast-in-situ joint region. Confining reinforcement in the form of transverse bars and vertical shear studs is also installed in the joint. The paper describes a series of tensile tests which were carried out to simulate the tensile zone of a joint loaded in pure flexure. The headed bars used in the tests were 25mm in diameter with 70mm square heads and yield strength of 530MPa. The tests studied the influences of concrete strength, headed bar spacing, splice length, transverse reinforcement and confining shear studs on joint strength. A lap length of 100mm in concrete with 28MPa cylinder strength was found to be sufficient to develop the full strength of the headed bars. A strut-and-tie model (STM) is presented for determining joint strength. Analysis shows that the STM gives safe results even though it does not fully capture the observed joint behaviour. An upper bound plasticity model is found to give relatively good predictions of joint strength in most cases, although it also does not always capture the correct failure mechanism. The tests provide insights into joint behaviour which, in conjunction with numerical modelling, will facilitate the development of an improved design method. Widespread use of this system would lead to improvements in buildability, sustainability and health and safety in the construction of concrete structures.

Keywords: Precast concrete, Headed reinforcement, Lap length, Strut-and-tie, Plasticity.

Notation

α	Angle between the diagonal strut and the transverse bar axis

γ_c	Partial safety factor for concrete
γ_s	Partial safety factor for steel reinforcement
θ	Angle of line drawn between centrelines of opposite heads to line normal to headed bars
ν	Effectiveness factor for concrete
σ_2	Confinement pressure
$\sigma_{tr,\ measured}$	Measured transverse bar axial stress at failure
$\sigma_{tr,\ pred\ test}$	Predicted transverse bar axial stress at the measured joint failure load
Φ_T	Transverse reinforcement mechanical ratio
$\emptyset_b$	Bar diameter
$\emptyset_{hb}$	Headed bar diameter
$\emptyset_{stud}$	Shear stud diameter
$\emptyset_{sh}$	Shear stud head diameter
$\emptyset_{tr}$	Transverse bar diameter
$A_{confinement}$	Confined concrete area
A_{hb}	Headed bar cross-sectional area
$A_{s,tr}$	Total transverse bar cross-sectional area
A_{tr}	Transverse bar cross-sectional area
D_{hb}	Diagonal length between adjacent headed bars
E_s	Reinforcement elastic modulus
L_{hb}	Headed bar lap length between bearing faces of heads
N_{hb}	Force applied to central headed bar
N_{tr}	Force in transverse bar
N_{strut}	Force in diagonal concrete compressive strut
$N_{u,\ joint}$	Joint capacity
$N_{u,\ strut}$	Concrete strut capacity
$N_{y,hb}$	Headed bar yield load
$N_{y,tr}$	Transverse bar yield load
P_{STM}	Predicted STM failure load
P_{test}	Maximum load achieved in test
P_{UB}	Predicted upper bound failure load

S_{hb}	Spacing of headed bars with same orientation
a	Projected length of diagonal failure plane in transverse direction
b_{hb}	Head size of headed bar
b_{strut}	Diagonal concrete strut width
c_{hb}	Cover to headed bar
c_{stud}	Cover to stud head
$f_{c,cyl}$	Measured concrete cylinder compressive strength
f_{ck}	Characteristic concrete cylinder compressive strength
$f_{ck,c}$	Characteristic confined concrete cylinder compressive strength
f_{ct}	Measured concrete tensile strength
f_u	Measured reinforcement ultimate stress
f_y	Measured reinforcement yield stress
$f_{yk,\,hb}$	Headed bar characteristic yield stress
$f_{yk,\,tr}$	Transverse bar characteristic yield stress
h_{conf}	Perpendicular distance from headed bar centreline to the underside of shear stud
$h_{strut,c}$	Confined strut depth
h_{stud}	Depth of confined concrete strut
n_{tr}	Number of transverse bars contributing to the tie in the STM
r	Coefficient in upper bound model
t_{stud}	Thickness of stud head
x_t	Transverse bar offset from the centreline of the joint

1. Introduction

In precast concrete construction, satisfactory design of connections between individual elements is crucial for ensuring overall strength and robustness. Many methods can be adopted to connect precast concrete elements including, amongst others, welded connections, grouted dowels and in-situ stitches. The optimum choice of connection method is strongly influenced by the forces that need to be transferred between precast elements. The paper addresses the design and behaviour of narrow cast in-situ joints between precast concrete elements in which continuity of reinforcement is achieved through overlapping

headed bars. The use of headed bars can achieve a full strength joint in tension, while significantly reducing the lap length compared to traditional straight bar laps. This type of connection has many practical applications. For example, it is used by Laing O'Rourke in their patented E6 floor system to form a continuous concrete floor by connecting precast concrete floor planks within the floor depth. The use of precast elements separated by narrow joints allows a very efficient construction process in which the planks are temporarily connected by steel brackets until the joint concrete has cured, eliminating the need for traditional propping and facilitating an extremely rapid construction programme for the structure, installation of other manufactured elements, and follow-on trades. Since the joints lie within the slab depth, storey heights can be minimised when compared to other types of precast concrete construction.

The heads used in this study are large enough to develop the full yield strength of the bar by bearing at the head, without any contribution from bond along the bar. The headed bars in adjoining precast slabs are placed out of phase by half the bar spacing as shown in Figure 1. Transverse bars and confining vertical shear studs are installed prior to concreting the joint which is designed using a strut-and-tie model (STM) to fail by yielding of the headed bars. The paper presents the results of an experimental programme carried out at Imperial College London to obtain a better understanding of the mechanical behaviour of tension splices using headed bars. The tests investigate the influence of transverse reinforcement, confining shear studs and concrete strength on joint strength and ductility. The test results are used to assess a STM of the joint developed by Laing O'Rourke and Arup.

2. Previous Studies

Headed bars are anchored through a combination of bond and bearing at the head with tests showing that the full bar strength can be developed at the head when it has a net bearing area of nine times the bar diameter [1]. According to the Canadian Code CSA A23.3-14 [2] bars with a head area equal to ten times the bar area are "deemed capable of developing the tensile strength of the bar without crushing of the concrete under the head provided that the specified concrete compressive strength is equal to or greater than 25MPa and the yield strength of the bar used in the design does not exceed 500MPa". There have been several previous studies into headed bar joints [3-7] mainly focussed on bridge deck applications. Thompson et al. [3,4] developed a model for the resistance provided by head bearing based on

recommendations given in ACI 318-02 [8] for side-blowout and bearing strength. Due to small head sizes, most of the bars used in their studies required a contribution from the bonded length to develop the full bar strength. The model [3] is applicable for anchorage lengths of at least six times the bar diameter which is greater than the anchorage of four times bar diameter provided in the majority of tests reported in this paper. Although Thompson et al. tested some specimens with additional transverse reinforcement, the beneficial effect of this is not considered by their model. The effect of transverse reinforcement was later investigated by Chun [5], who conducted tests on beams with headed bar lap splices under four-point bending. Most of Chun's tests were done using 29mm diameter bars with a head bearing area of four times the bar area, and lap lengths varying from 435mm to 870mm. He concluded that providing transverse reinforcement in the form of stirrups increased anchorage strengths by up to 67% and restrained prying action of the headed bars resulting from curvature of the beam.

Li et al. [6] conducted bending tests on slabs with overlapping 16mm bars with 13mm thick, 51mm diameter circular friction welded heads capable of developing the full bar strength. The headed bar spacing in the precast units was either 102mm or 152mm and the lap was varied between 64mm and 152mm. Concrete strengths varied from 53MPa to 72MPa. Two 16mm bars with 35mm circular heads at each end were placed transversely across the specimen at the centre of the joint, one above and one below the overlapping headed bars. In order to develop a full strength joint in which reinforcement yielded before concrete crushing, the authors recommend a minimum lap length of 152mm. Li et al. [7] also investigated the influence of fatigue loading on headed bar splice joints and concluded it had no effect on joint strength after 2, 000, 000 load fatigue cycles. However, the fatigue cycles reduced ductility significantly. In a follow-up publication, Li and Jiang [9] developed a schematic strut-and-tie model to predict joint strength in which strut strengths are calculated in accordance with ACI 318-11 [10]. The model gives safe and conservative predictions for all their tests but is not rigorous since equilibrium is not satisfied at all nodes.

The above studies provide insight into the anchorage of headed bars in lap splices but are not directly applicable to the short headed bar tension splices considered in the present research.

3. Test Specimen Development and Strut-and-Tie Model

Figure 2 shows the forces acting on a headed bar splice joint loaded in pure flexure. This paper describes a series of tension tests that were carried out to investigate the strength of such joints. The test specimens were designed to simulate the transfer of tension between headed bars in the dashed zone indicated in Figure 2. The heads used in this study are sufficiently large that the full tensile strength of the bar can be developed at the head without the need for bond along the bar. Therefore, tension is assumed to be transferred between the overlapping reinforcement bars through a series of diagonal concrete struts as shown in Figure 3. For equal bar forces, bar spacing and correct alignment of heads, transverse components of force in diagonal struts are balanced at bar heads with the exception of the last headed bar where transverse reinforcement is needed for equilibrium.

In the current research, the smallest possible joint configuration of a three bar splice (Figure 4), was tested for ease of construction, loading and numerical modelling. A limitation of the tested joint configuration is that it does not simulate prying action arising from flexural deformation. Consequently, the authors also carried out a series of comparative four point bending tests on 600 mm wide by 300 mm thick slabs with headed bar tension splices with the same bar spacing and lap length as shown in Figure 4. The strength of the splice joints in the bending tests was found to be greater than measured in comparable tension tests [11]. This could be because the three bar arrangement used in the tension tests induces in-plane bending which is restrained by the adjoining precast elements in flexural tests. The greater strength of the tension splices in the flexural tests also suggests that prying action had minimal effect on joint strength for the short lap lengths tested in this study. This is not the case for longer laps like those used by Chun [5] where prying action can significantly reduce lap strength.

Figure 5 shows a STM developed by Laing O'Rourke and Arup for the three bar arrangement used in this study. The model was calibrated using data from a series of unpublished tests on tension specimens carried out at the Building Research Establishment (BRE) UK. The aim of the current test programme was to investigate parameters not considered in the BRE tests. The height of the central node is assumed to be $0.4(L_{hb}/2 + x_t)$, where L_{hb} is the lap length between the insides of the heads, and x_t is the eccentricity of the transverse bar from the centreline of the joint (see Figure 5). The diagonal struts are assumed to be parallel sided. The T and B transverse bars in Figure 4 are neglected in the STM. For square heads and

symmetrical joint geometry with no offsets in reinforcement positions, the strut width perpendicular to its centreline is given by:

$$b_{strut} = 0.5b_{hb}sin\ \alpha + 0.4(\frac{L_{hb}}{2} + x_t)cos\ \alpha \quad (1)$$

where b_{hb} is the width of the head, x_t is eccentricity of the transverse tie from the joint centreline and α is the angle between the diagonal strut and the transverse bar axis which is given by:

$$tan\alpha = \frac{0.8(0.5L_{hb} + x_t)}{0.5S_{hb} - 0.25b_{hb}} \quad (2)$$

where S_{hb} is the spacing of headed bars with same orientation.

The strut and tie forces N_{strut} and N_{tr}, respectively, are given by:

$$N_{strut} = {}^{N_{hb}}/_{2\sin\alpha} \text{ and,} \quad (3)$$

$$N_{tr} = {}^{N_{hb}}/_{2\tan\alpha} \quad (4)$$

where N_{hb} is the force applied to the central headed bar.

The bearing stress under the heads is not checked because the head size is sufficient to develop the full bar strength. The diagonal strut strength equals the product of its cross sectional area, which is assumed constant, and the effective concrete strength. In reality, the strut is bottle shaped and the effective concrete strength varies along its length because of the diminishing effect of confinement with distance from the nodes. In the STM, the strut cross sectional area is calculated at the nodes, where the concrete strength is enhanced by confinement. Consequently, the effective concrete strength of the diagonal strut is enhanced to compensate for calculating its strength in terms of the head size as suggested by Tuchscherer et al. [12].

The strut depth and effective concrete strength are assumed to depend on whether or not transverse shear studs are present. In the absence of shear studs, the strut depth is taken as the head depth b_{hb} , as assumed by Li and Jiang [9] and the concrete strength is taken as the characteristic cylinder strength f_{ck} compared with 0.85 f_{ck} assumed by Li and Jiang [9]. The strut strength is assumed to be increased by the confinement provided by out-of-plane transverse shear studs, and in-plane headed bars. Where present the longitudinal confinement is assumed to be provided by the T and B transverse bars which are not

included in the STM. The characteristic confined concrete compressive strength, $f_{ck,c}$ is calculated with equation (5) from BS EN 1992-1-1:2004 [13].

$$f_{ck,c} = \min (f_{ck} + 5\,\sigma_2, 1.125\,f_{ck} + 2.5\,\sigma_2) \quad (5)$$

The confining pressure, σ_2 is calculated by dividing the yield strength of the shear stud by the hatched area, $A_{confinement}$, defined in Figure 6a since this is the smallest of the confining reinforcement. Figure 6b, which is drawn along the diagonal A-A in Figure 6a, depicts the calculation of the confined strut depth. The confining pressure is assumed to disperse from the shear stud head at a slope of 2 horizontal: 1 vertical as recommended for bearings in ACI 318-14 [14]. In cases where the resulting confined strut depth $h_{strut,c}$ is less than the head depth, the head is assumed to provide the same confinement within a 2:1 slope as shown in Figure 6b. Concrete that falls outside of the confined strut is conservatively considered not to contribute to strut strength. In some cases, the capacity of an unconfined strut with depth equal to the head size, b_{hb}, can be greater than a shallower confined strut. Consequently, the design strut capacity is defined as:

$$N_{u,\,strut} = \max \begin{cases} f_{ck,c}\, b_{strut}\, h_{strut,c}/\gamma_c \\ f_{ck}\, b_{strut}\, b_{hb}/\gamma_c \end{cases} \quad (6)$$

where γ_c is the partial factor for concrete which is taken as 1.5 for design but 1.0 in the strength assessments of this paper. For symmetrically positioned shear studs, the confined strut depth $h_{strut,c}$ is calculated from geometry as:

$$h_{strut,c} = 2 \times \min(0.5 b_{hb}, 0.5 h_{conf} + \frac{\emptyset_{sh}}{8} + \frac{b_{hb}}{4} - \frac{D_{hb}}{8}) \quad (7)$$

where h_{conf} is the perpendicular distance from the centreline of the headed bar to the underside of the shear stud, $\emptyset_{sh}$ is the head diameter of the shear stud and D_{hb} is the length of the diagonal A-A in Figure 6a. In the case of asymmetrically positioned shear studs, the upper and lower confined strut depths can be unequal as shown in Figure 6b. Theoretically, bending is introduced into the headed bar if the upper and lower strut depths are unequal. The effect of this is negligible for the test results presented in this paper due to the inherent conservatism of the STM.

The joint strength is limited by the diagonal concrete strut, transverse bar, or headed bar as follows:

$$N_{u,joint} = \min \begin{cases} 2\, N_{u,strut} \sin\alpha \\ 2\, n_{tr}\, A_{tr}\, f_{yk,tr} \tan\alpha\, /\gamma_s \\ A_{hb}\, f_{yk,hb}/\gamma_s \end{cases} \quad (8)$$

where n_{tr} is the number of transverse bars contributing to the tie at the top of the joint, A_{tr} and A_{hb} are the cross-sectional areas of the transverse bars and headed bars respectively, and $f_{yk,tr}$ and $f_{yk,hb}$ are the characteristic yield stresses of the transverse bars and headed bars respectively. γ_s is the partial factor for reinforcement which is taken as 1.15 for design but 1.0 in the strength assessments of this paper. As presented, the STM is applicable to laboratory controlled specimens; for construction applications a separate assessment would be required to validate the joint performance with relevant construction tolerances.

4. Upper Bound Plasticity Model

As an alternative to the STM, an upper bound plasticity model proposed by Joergensen and Hoang [15, 16] for U-bar splices is also considered. The only change to the model is that plane stress is considered instead of plane strain. This gives lower and more realistic strength predictions for the tested joints and is justified by the observation that the anchor plates are suggestive of a strut and tie system in plane stress. The member depth is assumed to equal to the head size of 70 mm as in the STM without shear studs. Concrete and reinforcement are assumed to behave in a rigid plastic fashion and dowel action is neglected. In plan, the failure mechanism is as shown in Figure 5b. No energy is dissipated in the separation yield lines shown in Figure 5b since the relative displacements are normal to the yield line. In this paper, the concrete effectiveness factor, ν, is taken as 1.0 due to the high confinement present and unlike the STM no increase in concrete strength is made when shear studs are present. For plane stress, the limiting upper bound equation is:

$$N_{u,joint} = \nu f_{ck} L_{hb} b_{hb} \left(\sqrt{r + \left(\frac{a}{L_{hb}}\right)^2} - \frac{a}{L_{hb}} \right) / \gamma_c \qquad (9)$$

where r = 1 for transverse reinforcement mechanical ratio $\Phi_T \geq 0.5\nu$. For lower values of Φ_T, r is given by

$$r = 4\frac{\Phi_T}{\nu}\left(1 - \frac{\Phi_T}{\nu}\right) \qquad (10)$$

$$\Phi_T = \frac{A_{s,tr}\, f_{yk,tr}}{L_{hb} b_{hb} f_{ck}} \qquad (11)$$

$$a = \frac{S_{hb}}{2} - b_{hb} \qquad (12)$$

$A_{s,tr}$ is the total cross-sectional area of the transverse bars provided. The partial factor for concrete, γ_c, is taken as 1.0 in the strength assessments of this paper as for the STM.

The coefficient r is 1 for all the specimens in this study.

5. Experimental Testing

5.1. Test Specimen Details

Twenty seven specimens were tested of which twenty one had the geometrical arrangement shown in Figure 4 which is the same as used by Laing O'Rourke in their E6 system. The standard E6 lap length, between the inside face of the heads, and bar spacing are 100mm and 200mm respectively. Six further tests investigated the influence of varying the headed bar spacing and lap length. Other variables were concrete strength, transverse bar size and arrangement and the presence or absence of shear studs. The headed bars were 25mm in diameter with standard 70x70x16mm friction welded square heads. Their length was 400mm, measured between the inside faces of the heads. Where present, two 10mm diameter 125mm long shear studs were placed at the positions shown in Figure 4. The cover to the stud head c_{stud} was zero, the stud head diameter was 30mm and the stud head thickness t_{stud} was 2mm (see Figure 6). The 36mm spacing of the transverse bars shown in Figure 4 was chosen to allow sufficient space for concrete to be placed in contact with the bar heads and to allow clearance for the friction weld flash. The specimen length was chosen to provide adequate anchorage for bond failure of the transverse bars not to limit the failure load of the connection. For reference, the predicted transverse bar force at headed bar yield is 200kN. The tests focussed on concrete controlled failures with a view to determining the critical concrete strength at which bar yield precedes concrete failure, and to better observe the effect of other variables on joint performance. Table 1 summarises the details of the tested specimens which are divided into five groups, with the test ID describing the specimens as follows:

For example, G4-39-2H20:TT'-S-100-250:

" G4 " – Test group

" 39 " – Measured concrete cylinder strength at time of testing

" 2H20 " – Number and diameter of transverse bars

" TT' " – Position of transverse bars as indicated in Figure 4

" S " – Shear studs included

" 100 " – Lap length of headed bars

" 250 " – Spacing of headed bars

Group 1, with shear studs, and group 2, without, investigated the influence on joint strength of transverse bar diameter and concrete strength. The transverse bars were positioned at the T and T' locations (see Figure 4) as in the Laing O'Rourke E6 joint. The B and B' bars are time consuming to fix in practical joints. Groups 3 to 5 respectively varied the spatial arrangement of transverse bars, the spacing of headed bars and the lap length of headed bars. In group 5, the centreline of the transverse bars was positioned 32 mm from the inside face of the heads as shown in Figure 4. Consequently, the spacing of the transverse bars varied with the lap length. Concrete compressive and tensile strengths were measured from control specimens cured in the same conditions as the joint specimens, and tested at the same time. Compressive strength tests were performed according to BS EN 12390-3:2009 [17] using 200mm high cylinders with a diameter of 100mm. Splitting tests to determine tensile strength were performed according to BS EN 12390-6:2009 [18] on 300mm high cylinders with a diameter of 150mm. At least three specimens of each type were tested. Reinforcement material properties were derived from coupon tension tests according to BS EN ISO 6892-1:2009 [19]. Three specimens of each bar type were tested with average results given in Table 2. Stress-strain curves for the 25mm headed bar coupon tests are presented in Figure 7, wherein strains were measured with strain gauges and stresses calculated with a cross-sectional bar area of 490.9mm^2.

5.2. Test Setup and Instrumentation

A servo-hydraulic controlled internal reaction frame was used to load the specimens in uniaxial tension under displacement control with a load rate of 0.2mm per minute. Load was applied continuously up to failure. The ends of the headed bars were clamped to the test rig by means of specially fabricated 50mm thick steel plates with 25mm thick slots to accommodate the reinforcement heads (Figure 8). Rapid setting resin was applied to the heads of the bottom headed bars before the bottom plates were secured in position to allow for any misalignment of the friction welded heads.

The outputs gathered from the test rig were the load and platen-to-platen displacement. Several strain gauges were fixed to the reinforcement inside the concrete. Figure 9 shows the arrangement of strain gauges used, mostly with the aim of capturing bending and axial forces in the transverse reinforcement, though not all specimens were fully gauged. Additionally, a digital image correlation, or D.I.C. system was

used to monitor cracking in the face parallel to the plane of the headed bars with minimum cover (see Figure 4 Section A-A). A random speckle pattern was sprayed onto the surface of the specimen such that the LaVision StrainMaster system [20] could track the movement of the pattern on the specimen by comparing images at different load stages. Two high resolution cameras captured images of the surface of the specimen in stereo mode every 3 seconds. Since two cameras were used, it was possible to capture 3D displacements, surface strains and crack propagation.

6. Results and Observations

The measured and calculated STM and upper bound strengths of the tested specimens are listed in Table 1 which also gives the actual and predicted failure modes. These are discussed further below. The yield strength of the headed bars was 260kN. Test failures are classified as Joint (J) when joint failure occurred before or at headed bar yield due to concrete failure alone or in combination with partial yielding of the transverse bars, and Headed bar (H) when extensive yield of the headed bar occurred prior to eventual joint failure. Results for the upper bound model are classified in a similar manner, where joint failure (J) corresponds to failure in the assumed yield lines. Failure loads were calculated with measured material strengths instead of characteristic strengths and partial material factors of 1.0. The maximum calculated resistance was limited to the ultimate strength of the headed bars. The failure modes of the STM are defined according to the limiting mode calculated with equation (8). Predicted failure loads for the specimens in this study were lower than the headed bar yield load in all cases and are denoted (S) for strut failure and (T) for tie failure. Table 1 shows that the STM gives conservative predictions of joint strength in all cases but there is significant scatter in the results which is discussed later. The upper bound model gives good strength predictions which are typically greater than the STM predictions as expected. The test results are discussed in detail below for each group.

6.1. Test Groups 1 and 2 Results

6.1.1. Load-displacement response

Load-displacement results are presented in Figure 10 for group 1 with shear studs, two transverse bars of varying diameter and concrete strengths of 26MPa, 40MPa and 54MPa. An average load-displacement curve for bare bars from the headed bar tensile tests is also included. Since the tensile tests were on bars

of the same length as used in the standard tests, the bare bar curve was calculated by adding the displacements of the fully loaded bar to those of the same bar with half the applied load. It should be noted that the overall measured extension of both bare and concrete encased bars was slightly increased by deformation of the clamped heads with differences between the two due to concrete deformation. Figure 10 shows that the axial deformations of the bare and concrete embedded bars are similar prior to commencement of joint failure for concrete strengths greater than 40MPa. The joint strength reached the yield strength of the headed bars in tests G1-54-2H16:TT'-S-100-200, G1-54-2H20:TT'-S-100-200 and G1-48-2H25:TT'-S-100-200 but with the exception of G1-54-2H20:TT'-S-100-200 ductility was limited by joint failure. Table 1 shows that the STM, unlike the upper bound model, significantly underestimates the strength of joints with 2H16 transverse bars where failure is predicted to occur due to yielding of the T' bar. This is because the STM neglects the contribution of the T bar which resists significant force as discussed below. Table 1 also shows that the STM gives conservative estimates of joint strength where limited by strut strength.

Figure 10 shows that the initial stiffness of joints with shear studs was similar up to around 60kN irrespective of concrete strength and transverse reinforcement area. The stiffness of joints with 26MPa concrete reduced upon further loading but the stiffness of specimens with concrete strengths of 40MPa and 54MPa remained almost constant until near failure. Specimens with concrete strengths of 40MPa and 54MPa failed more suddenly than for 26MPa concrete. The transverse bar diameter had little effect on joint stiffness and post-peak response except for specimens with 54MPa concrete where the failure mode changed from joint to headed bar yielding when the transverse bar diameter was increased from 16mm to 20mm. Comparison of Figures 10 and 11 shows that the post-peak response was notably more brittle for specimens without shear studs but prior to failure the response of specimens with and without shear studs was similar.

Figure 12 shows the influence on joint strength of concrete strength and transverse bar diameter with and without shear studs. The strength of comparable specimens increased with concrete strength and the provision of shear studs. Joint strength increased slightly when the transverse bar diameter was increased from 16mm to 20mm. The increment in strength increased with concrete strength and was greatest for specimens without shear studs. However, the strength of specimens with H25 transverse bars was comparable to that of similar specimens with H16 transverse bars.

6.1.2. Reinforcement forces

Comparison of the applied load and bar force at gauges S1 and S5, adjacent to the head (see Figure 9), indicates that bond along the embedded length of the headed bar became insignificant at around 75kN for concrete strengths of 26MPa, and between 125kN to 150kN for the higher strengths. Bending moments at the head were low and of variable sign, gradually increasing with applied load, but generally not exceeding 10% of the plastic moment capacity.

Figure 13 shows an axial load-bending moment interaction diagram for the transverse bars in group 1. These were calculated considering an idealised elastic-plastic stress-strain curve since the reinforcement had a well-defined yield plateau and measured strains did not approach the strain hardening region. Results are shown at gauges S2-S3 on the T' bar and S8-S9 on the T bar (see Figure 9) of which only the T' bar is assumed to contribute to joint strength in the STM. Significant bending moments developed at failure in both the T and T' transverse bars with the exception of the T' bar in specimens G1-40-2H16:TT'-S-100-200 and G1-54-2H16:TT'-S-100-200 where the bars were close to yielding in tension. Transverse bars larger than 16 mm diameter did not reach their yield strength irrespective of the concrete strength. Tensile forces in the T bars at gauges S8-S9 were typically around 40% to 50% of those in the T' bar at gauges S2-S3 but the bending moments were similar particularly for 16mm transverse bars. Bending moments were proportionately greater in specimens with the lowest concrete strength of 26MPa.

Strain gauge data show no correlation between shear stud stress and concrete cylinder strength or transverse bar size. Tensile stresses in shear studs were generally below 50% of yield at ultimate joint strength with the exception of specimen G1-48-2H25:TT'-S-100-200 with 25mm transverse bars, where the stress approached 90% of yield.

6.1.3. Crack development and failure mechanism

DIC was used to continuously determine crack widths and surface principal strains. Figure 14 shows surface principal strains for two typical tests at failure. Regions of high strain correspond to cracks. Figure 15 shows the crack pattern at failure in the front face of test specimen G1-40-2H20:TT'-S-100-200 which is typical. Crack 1 formed first at the top of the specimen, due to bending induced by the three bar arrangement, and propagated downwards along the central headed bar. The crack appeared at around 25kN in specimens with 26MPa concrete, and at around 45kN for concrete strengths of 40MPa or more. The V-shaped crack 2 formed next. It became visible at around 65kN in specimens with 26MPa concrete,

and at around 100kN to 150kN for greater concrete strengths. Crack 2 typically initiated near the head of the central headed bar and propagated upwards towards the outer ends of the supporting bar heads. Cracks 3 and 4 typically occurred as failure was approached, initiating close to the head of the supporting headed bars and propagating downwards towards the head of the central headed bar, sometimes joining up with crack 1 or 2. Failure was typically accompanied by widening of cracks 3 and 4, along with pull-out of a central cone of concrete between the supporting headed bars.

Removal of loose concrete after testing suggests that the central headed bar slips over the transverse bars at failure, rather than pulling out a cone of concrete of the full specimen depth. Such a failure mechanism is also consistent with the observed spalling of concrete cover at the head of the central headed bar towards the end of most tests. These failure planes are depicted in a simplified manner in Figure 16 which has considerable similarities with the upper bound failure mechanism shown in Figure 5b. Figure 17 shows typical specimen photos after removal of loose concrete and the central headed bar, revealing analogous failure planes. Cracks at the back of specimens were significantly flatter than in the front face due to the non symmetrical failure mode shown in Figure 16.

6.2. Test Group 3 Results

Figure 18 shows load displacement plots for group 3 which investigated the influence of transverse bar arrangement. Providing transverse bars at positions T' and B' in Figure 4 rather than T and T' as in groups 1 and 2 significantly improved joint behaviour as predicted by the STM due to doubling of the tie resistance. However, the STM significantly underestimates diagonal strut strength as seen for specimen G3-28-2H20:T'B'-S-100-200 which failed at 236kN compared with 142kN predicted by the STM. The STM also neglects the benefit of having transverse reinforcement above and below the headed bar. For example, specimen G3-48-1H25:T'-S-100-200 with only one 25mm transverse bar failed in a brittle fashion at 243kN whereas specimen G3-46-2H16:T'B'-S-100-200 with two 16mm diameter bars failed after extensive plastic deformation at 316kN . According to the STM, both specimens should fail at a similar load because in both cases the transverse bar area and anchorage length is sufficient for headed bar yield.

Further enhancement in joint strength and ductility occurred when four transverse bars were provided with the headed bar yielding in tests G3-28-4H16:TT'BB'-S-100-200 and G3-28-4H20:TT'BB'-S-100-200 with concrete strength of 28MPa.

Strains in the headed bars show that, for all specimens in group 3, bond degradation occurs rather slowly with bond only becoming insignificant as the ultimate load is approached. Bending moments at the head are generally below 8% of the plastic moment capacity. Some specimens in this group had strain gauges fixed to both the T' and B' bars at the centre of the joint. In these cases, the forces in T' and B' bars were practically identical. Figure 19 shows transverse bar force interaction plots at gauges S2-S3 for the T' bar. The proportion of load resisted by bending increases with reducing concrete strength and increasing transverse bar diameter.

Shear stud stresses were below 50% of yield load for all specimens except G3-28-4H16:TT'BB'-S-100-200 and G3-48-1H25:T'-S-100-200, where axial stresses reached around 80% of yield at the ultimate load.

With the exception of specimen G3-48-1H25:T'-S-100-200 with a single transverse bar, pull out of the central headed bar was restrained by the top and bottom transverse bars which largely maintained the integrity of the concrete within the lap zone as shown in Figure 20.

6.3. Test Groups 4 and 5 Results

Groups 4 and 5 investigated the effect of varying the headed bar spacing and lap length. Two 20 mm diameter bars were provided at the T and T' locations. Figure 21 shows that joint strength increases with increasing lap length (dashed lines) and reduces with increasing headed bar spacing (solid lines). Figure 22 shows that the ultimate strength of specimens with identical concrete strengths increases with increasing inclination θ of a line drawn between the centrelines of opposite heads as predicted by the STM.

Strain gauges were only provided on the transverse bars at locations S2 and S3 in groups 4 and 5. Figure 23 shows the interaction between axial load and bending moment. In all cases, the transverse bars failed to reach their yield capacity and shear stud stresses were below 50% of yield at failure. In both groups of tests, the shear stud stress at failure increased with reducing strut angle. Crack patterns were generally similar to those observed for groups 1 and 2 as shown in Figure 24 for tests G4-39-2H20:TT'-S-100-300 (top) and G5-25-2H20:TT'-S-200-200 (bottom). A V-shaped crack developed around 100mm from the top of specimen G5-25-2H20:TT'-S-200-200 at about 100kN (Figure 24 bottom) due to the long embedment length of the headed bars.

7. Discussion

Figure 25 compares the measured, STM and upper bound failure loads in Table 1. The results are sorted in ascending order of failure load, and limited to the headed bar ultimate strength. Even with the adopted partial material factors of 1.0, the STM is safe in all cases but its accuracy is variable largely due to errors in the predicted failure mode. The ratio of the STM predicted to measured strength has a mean of 0.72, standard deviation of 0.125 and coefficient of variation of 0.173 compared with a mean of 0.93, standard deviation of 0.196 and coefficient of variation of 0.211 for the upper bound model. The upper bound model is reasonably accurate for the tested specimens but since $\Phi_T \geq 0.5\nu$ strengths of geometrically similar specimens are incorrectly predicted to be independent of the provided transverse reinforcement.

According to the STM, the minimum concrete strength for headed bar yield is 62MPa for group 1 and 80MPa for group 2. The corresponding concrete strength for the upper bound model is 50MPa. With partial factors of γ_c = 1.5 and γ_s = 1.15, the required concrete strength increases to 85MPa and 105MPa respectively for the STM and 75MPa for the upper bound model. Comparison with the test results shows both models are very conservative in this respect since headed bar yield occurred in specimens G3-28-4H16:TT'BB'-S-100-200 and G3-28-4H20:TT'BB'-S-100-200 with concrete strengths of 28MPa.

The conservatism of the STM largely arises from its underestimate of diagonal strut strength and neglect of the T and B transverse reinforcement which is only assumed to provide longitudinal confinement since it is not required for equilibrium in the assumed STM geometry. However, changing the position of transverse bars from T' and T in group 1 to T' and B' in group 3, significantly increased joint strength and ductility as predicted by the STM when transverse bar yield is critical. Figure 26 compares axial stresses in the transverse bars at failure derived from measured strains ($\sigma_{tr,\,measured}$) and calculated with the STM at the measured joint failure load ($\sigma_{tr,\,pred\,test}$). The STM bar stresses are significantly greater than observed for joints with T or T and B bars but the comparison is better for the group 3 specimens without T or B bars. Better bar stress predictions are also observed for group 5 tests with longer lap lengths. A limitation of the STM is that the prescribed geometry of the model makes the joint strength independent of concrete strength when failure is governed by yielding of the transverse tie. Other STM solutions with more optimised geometry could give closer predictions to the test results but possibly at the expense of added complexity.

Figure 27 illustrates the influence of transverse bar arrangement and concrete strength on joint strength by comparing the strengths of specimens in groups 1 and 3. Providing transverse bars in the T and B positions, which are neglected in the STM, enhances the contribution of bond over the embedded length of the headed bar and inhibits the failure mechanism shown in Figure 16 where the headed bar slips over the T and T' transverse bars.

Results from groups 1 and 2 show that shear studs enhance joint strength, but strains in shear studs were generally below 50% of yield. Figure 28 compares measured and calculated percentage increases in joint strength of comparable specimens with and without shear studs. The STM clearly overestimates the benefit of shear studs whilst underestimating the strength of both confined and unconfined struts.

Comparison of specimens in groups 1, 4 and 5 shows that joint strength and ductility generally increase as the diagonal angle θ as defined in Figure 22 increases, as found by Li et al. [6]. Increasing the lap length increases the contribution from bond, resulting in a more distributed crack pattern along the bar. The STM predicts strut and tie forces to reduce as the lap length is increased. However, the confined strut height (see Figure 6) reduces as the lap length is increased potentially offsetting the benefit of increasing lap length as for specimens G5-25-2H20:TT'-S-150-200 and G5-25-2H20:TT'-S-200-200 in group 5 with 150mm and 200mm laps, where the STM predicts joint strengths of 196kN and 192kN respectively compared with measured strengths of 213kN and 261kN. In comparison, the increased lap length is beneficial in the upper bound model as this results in an increased surface area of the yield line, giving identical predictions to the measured joint strengths for these two specimens.

8. Conclusions

This paper describes a series of tests carried out on headed bar tension splice joints at Imperial College London. Joints of the tested configuration are used in the E6 floor system developed by Laing O'Rourke. The tested specimens are intended to represent the tensile zone of an in-situ joint between precast flooring units loaded in flexure but do not simulate flexural prying action. The tests investigated the influence on lap strength of joint geometry, concrete strength, transverse reinforcement cross sectional area and arrangement and shear studs. A STM is proposed for the design of headed bar tension splices with transverse reinforcement. The test results show that the STM is generally conservative and safe to use, even though it does not always capture observed failure mechanisms. The upper bound model of

Joergensen and Hoang [15, 16] also gives reasonable estimates of joint strength but it does not fully capture the influence of transverse reinforcement on joint strength.

Key conclusions from the tests are:

a) Lap strength is limited by headed bar strength, transverse bar yielding or concrete failure,

b) Joint strength and ductility is significantly enhanced by placing transverse bars on both sides of the headed bars in the T' and B' positions rather than on one side in the T and T' positions,

c) A lap of 100 mm in concrete with 28 MPa cylinder strength was sufficient to develop the full strength of the headed bars in the tested tension configuration when four H16 transverse bars were provided in T, T', B and B' positions,

d) Increasing concrete strength increases lap strength when governed by concrete failure and can change the failure mode to headed bar yield,

e) Providing shear studs in the lap zone can increase joint strength and ductility,

f) Increasing lap length or reducing headed bar spacing can increase joint strength and ductility

The detailed test results will be used to inform the development of alternative design approaches to the STM which although safe is overly conservative for economic design. Taking the average of a lower and upper bound model is one possible approach. It is hoped that the understanding of joint behaviour gained in this research will promote the use of headed bar tension splices in precast concrete construction. More widespread use of precast concrete construction in conjunction with headed bar splices would improve buildability and quality control as well as reducing construction time, material waste and on-site labour resulting in safer construction sites.

9. Acknowledgements

This is a research project funded by Laing O'Rourke. The authors would like to thank Arup for their collaboration in this project. Thanks also to the technicians at the Structures Laboratory at Imperial College London, in particular Mr. Leslie Clark and Mr. Stefan Algar for their availability and assistance throughout the testing programme.

References

1. Brooker, O., *Use of Headed Bars as Anchorage to Reinforcement.* The Structural Engineer, 2013: p. 49-57.
2. CSA, *Design of Concrete Structures (CSA A23.3-14)*. 2014, Canadian Standards Association. p. 297.
3. Thompson, M.K., et al., *Lap Splices Anchored by Headed Bars.* ACI Structural Journal, 2006. 103(S29): p. 271-279.
4. Thompson, M.K., et al., *Anchorage Behaviour of Headed Reinforcement*. 2003, The University of Texas at Austin. p. 114.
5. Chun, S., *Lap Splice Tests Using High-Strength Headed Bars of 550 MPa (80 ksi) Yield Strength.* ACI Structural Journal, 2015. **112**(6): p. 10.
6. Li, L., et al., *Improved Longitudinal Joint Details in Decked Bulb Tees for Accelerated Bridge Construction: Concept Development.* Journal of Bridge Engineering, 2010. **15**(3): p. 327-336.
7. Li, L., Z. Ma, and R.G. Oesterle, *Improved Longitudinal Joint Details in Decked Bulb Tees for Accelerated Bridge Construction: Fatigue Evaluation.* Journal of Bridge Engineering, 2010. **15**(5): p. 511-522.
8. ACI, *Building Code Requirements for Structural Concrete (ACI 318-02) and Commentary (ACI 318R-02)*. 2002, American Concrete Institute Committee 318. p. 443.
9. Li, L. and Z. Jiang, *Flexural Behavior and Strut-and-tie Model of Joints with headed bar details Connecting Precast Members.* Perspectives in Science, 2016. **7**: p. 253-260.
10. ACI, *Building Code Requirements for Structural Concrete (ACI 318M-11) and Commentary*. 2011, American Concrete Institute Committee 318. p. 503.
11. Vella, J. P., Vollum, R. L. & Jackson, A. 2017. *Headed Bar Connections between Precast Concrete Panels Loaded in Bending*. fib Symposium 2017 High-tech Concrete: Where Technology and Engineering Meet! Maastricht, The Netherlands. fib. p. 8.
12. Tuchscherer, R., et al., Confinement of Deep Beam Nodal Regions. ACI Structural Journal, 2010. 107(S70): p. 709-717.
13. BSI, *Eurocode 2: Design of concrete Structures - Part 1-1: General Rules and Rules for Buildings*. 2004, British Standards Institution. p. 225.

14. ACI, *Building Code Requirements for Structural Concrete (ACI 318-14) and Commentary.* 2014, American Concrete Institute Committee 318. p. 520.
15. Joergensen, H.B. and L.C. Hoang, Strength of Loop Connections between Precast Bridge Decks Loaded in Combined Tension and Bending. Structural Engineering International, 2015. 25(1): p. 71-80.
16. Joergensen, H.B. and L.C. Hoang, Tests and Limit Analysis of Loop Connections between Precast Concrete Elements Loaded in Tension. Engineering Structures, 2013. 52: p. 558-569.
17. BSI, *Testing hardened concrete Part 3: Compressive strength of test specimens*. 2009, British Standards Institution. p. 22.
18. BSI, *Testing hardened concrete Part 6: Tensile splitting strength of test specimens*. 2009, British Standards Institution. p. 14.
19. BSI, *Metallic materials - Tensile testing - Part 1: Method of test at room temperature*. 2009, British Standards Institution. p. 76.
20. LaVision, *Product Manual for DaVis 8.2*. 2014, LaVision GmbH: Gottingen, Germany. p. 120.

Investigation of Headed Bar Joints between Precast Concrete Panels

List of Figures

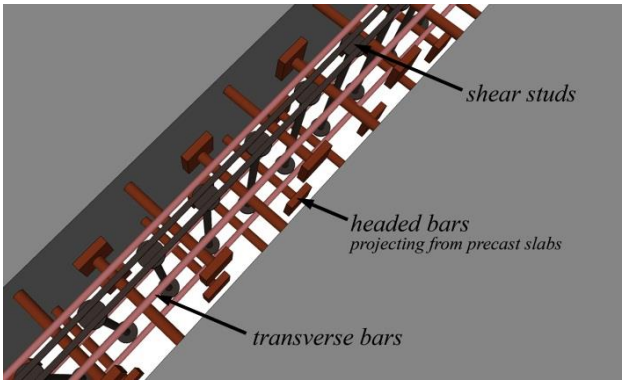

Figure 1: Typical headed bar joint

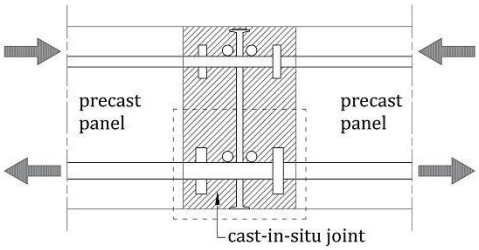

Figure 2: Forces acting on the joint location for a slab under bending (section)

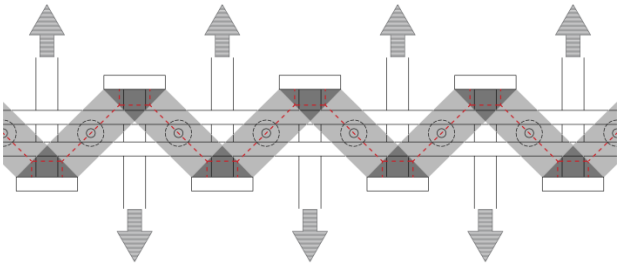

Figure 3: Tensile force transfer within headed bar joint (plan)

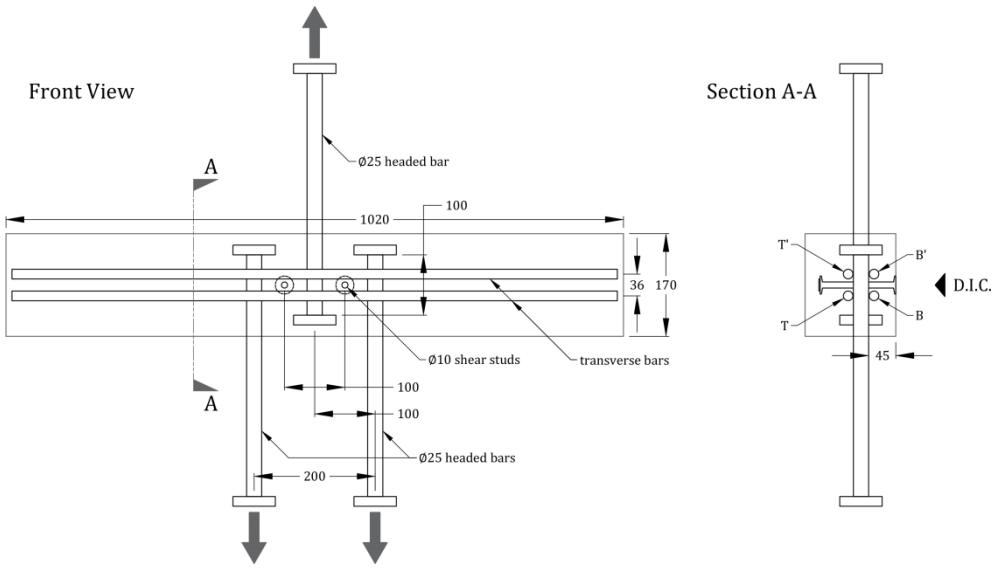

Figure 4: Typical test specimen

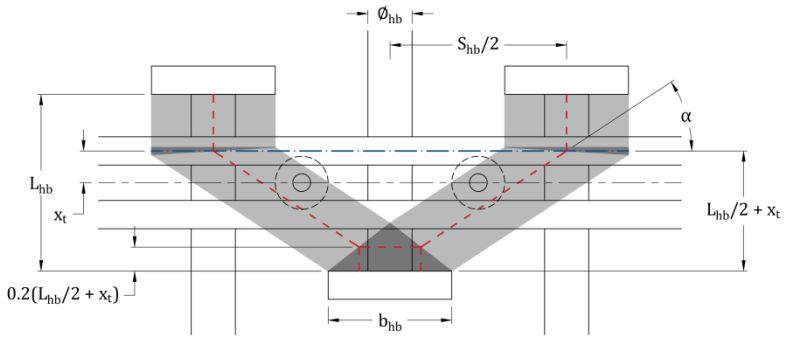

(a)

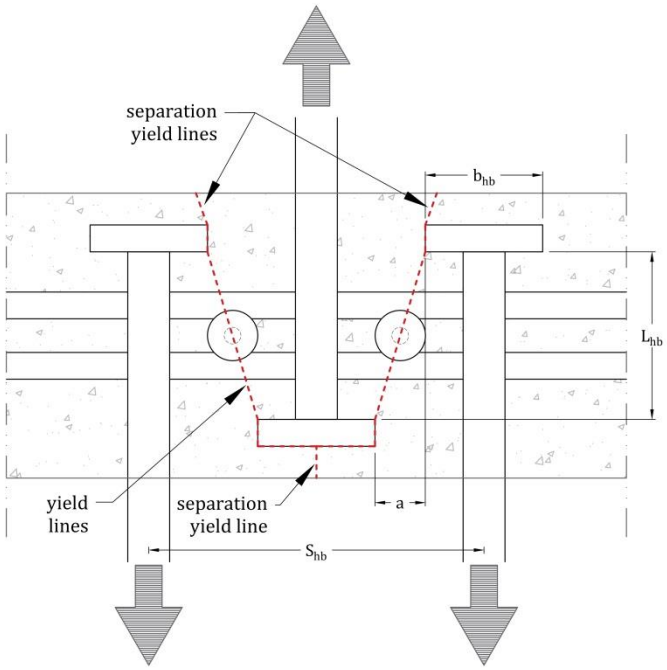

(b)

Figure 5: Design model for three-bar arrangement (a) STM and (b) and upper bound yield lines

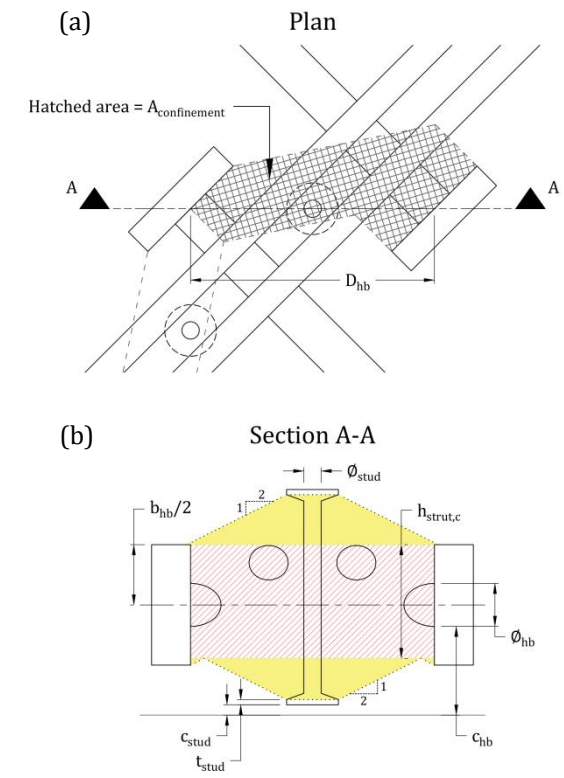

Figure 6: Effective confining area (a) and confined strut geometry (b)

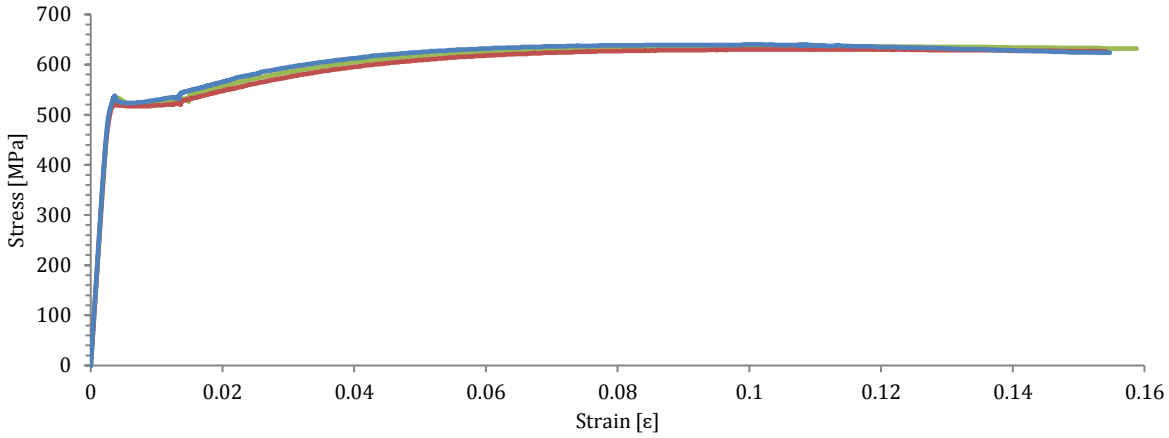

Figure 7: Stress-strain curves for 25mm headed bar coupon tests

Figure 8: Top reaction plates (left) and bottom reaction plates (right)

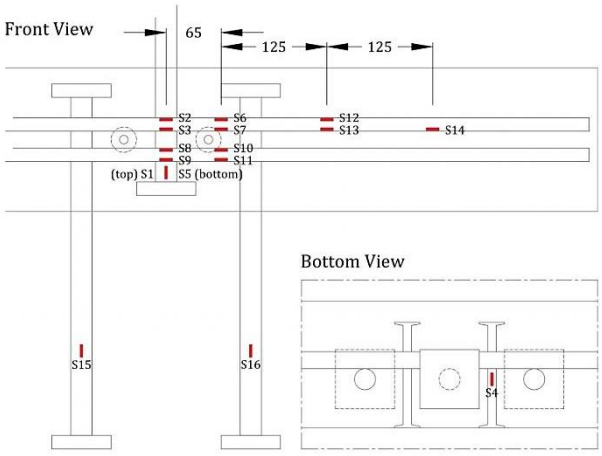

Figure 9: Strain gauge positions

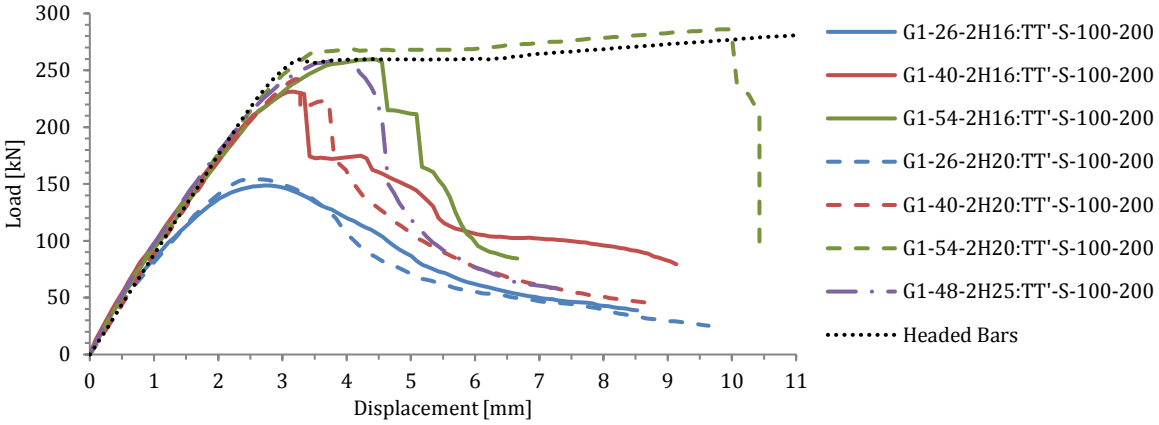

Figure 10: Test group 1 load-displacement

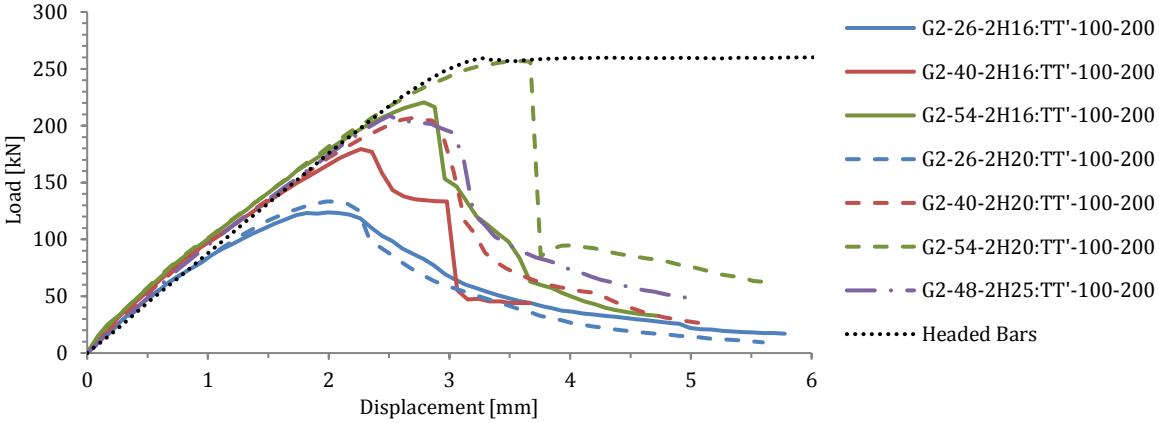

Figure 11: Test group 2 load-displacement

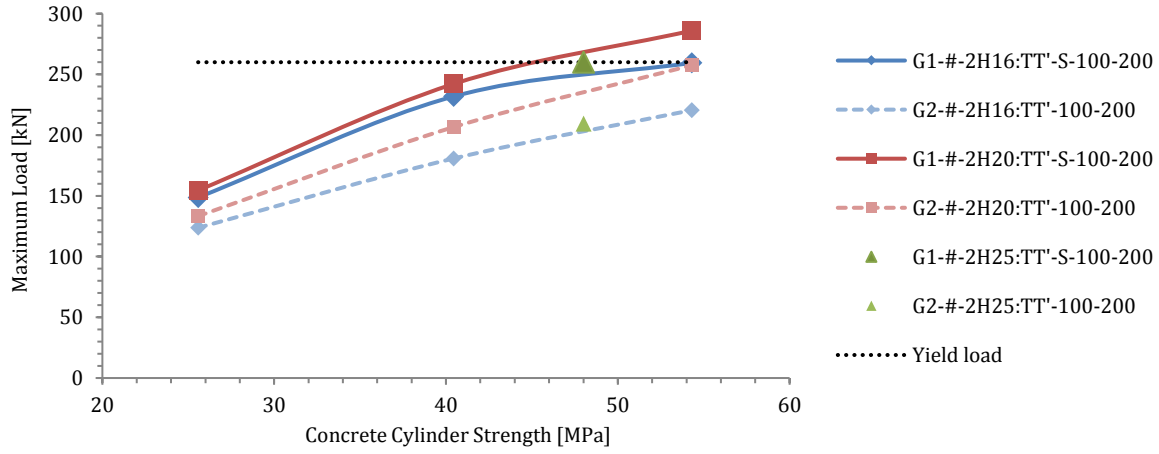

Figure 12: Test groups 1 and 2 comparison

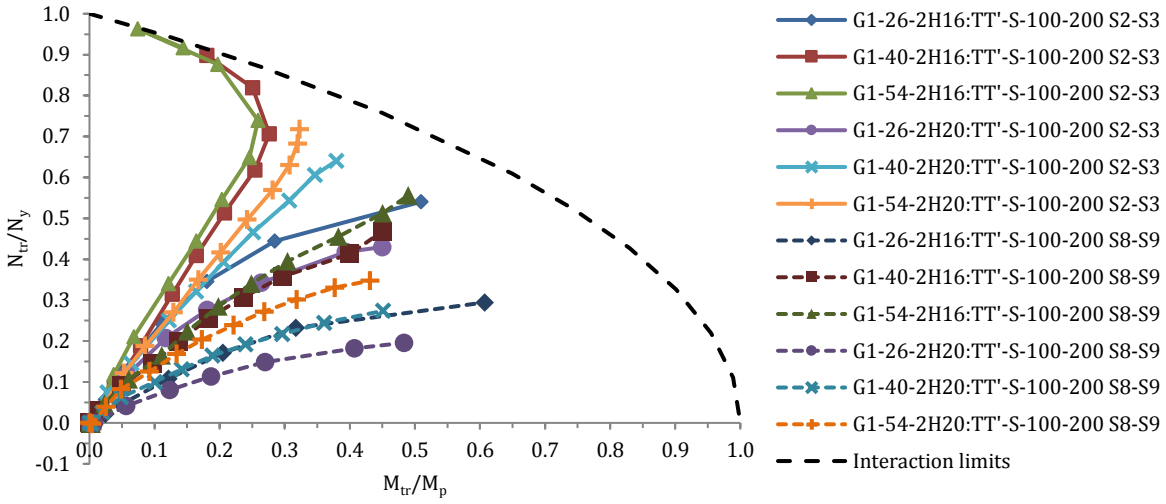

Figure 13: Test group 1 transverse bar force interaction

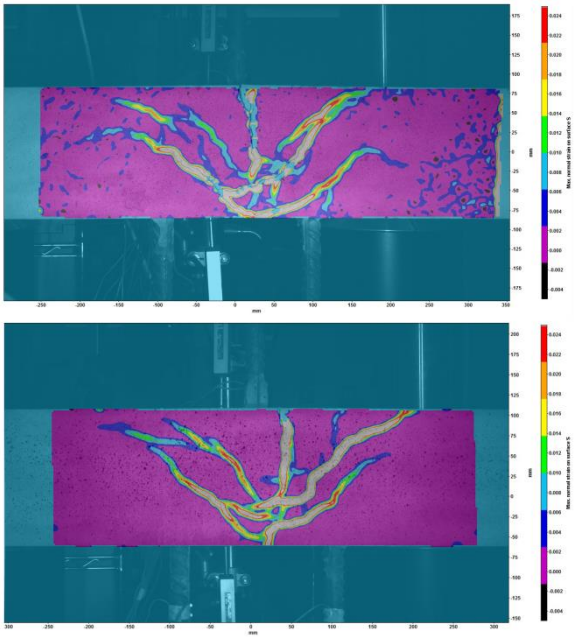

Figure 14: DIC processed images showing surface principal strains at failure: test G1-54-2H16:TT'-S-100-200 (top) and test G2-26-2H20:TT'-100-200 (bottom)

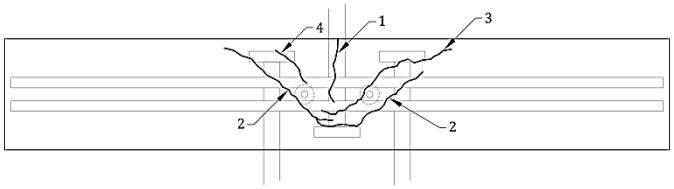

Figure 15: Test G1-40-2H20:TT'-S-100-200 crack pattern

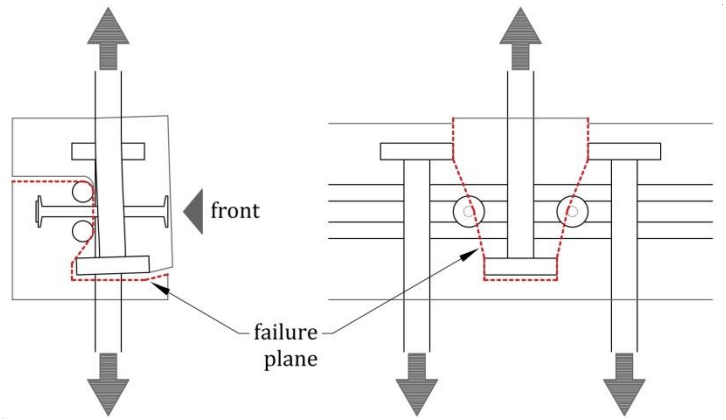

Figure 16: Simplified failure planes in section (left) and from front (right)

Figure 17: Typical specimen after removal of loose concrete (top) and central headed bar (bottom)

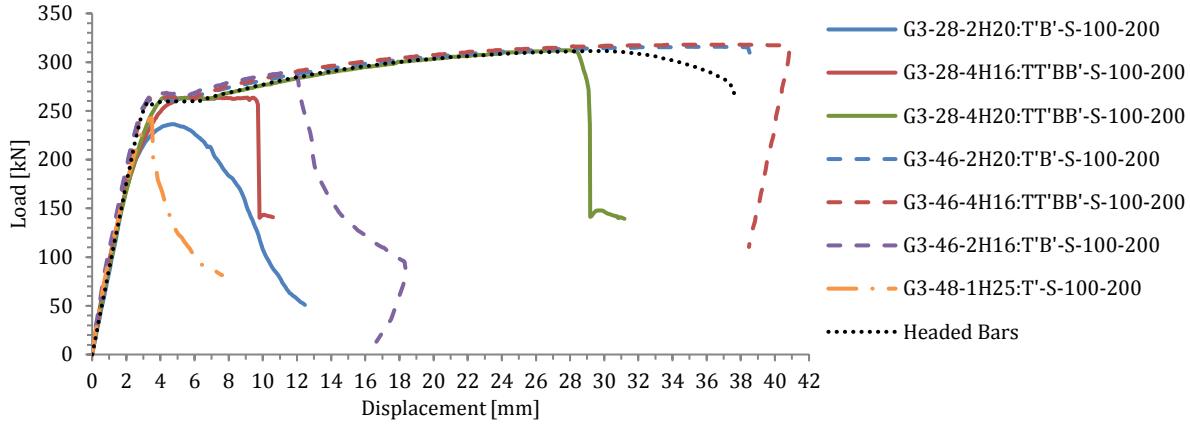

Figure 18: Test group 3 load-displacement

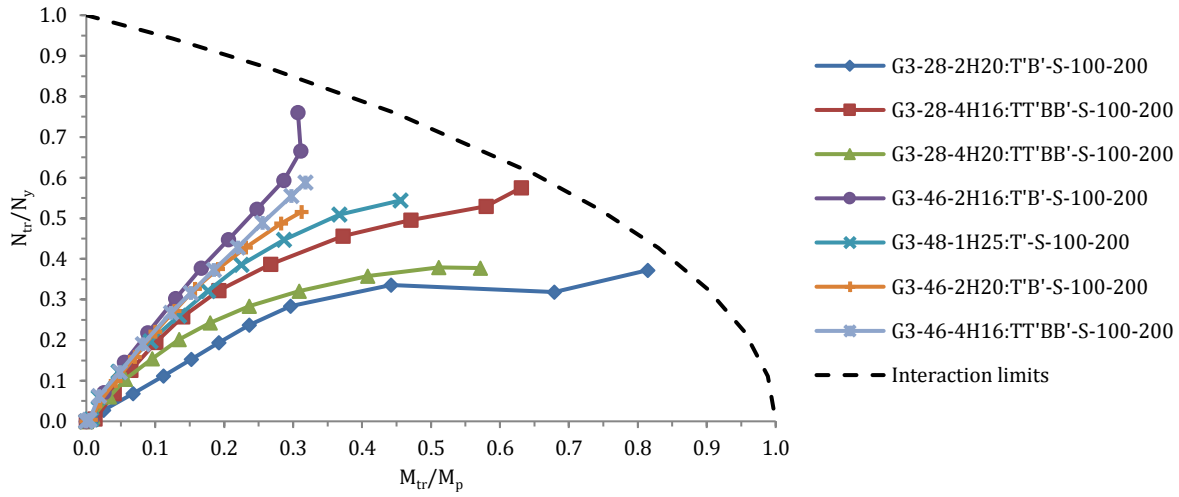

Figure 19: Test group 3 transverse bar force interaction at S2-S3

Figure 20: Specimen G3-28-2H20T'B'-S-100-200 after removal of loose concrete

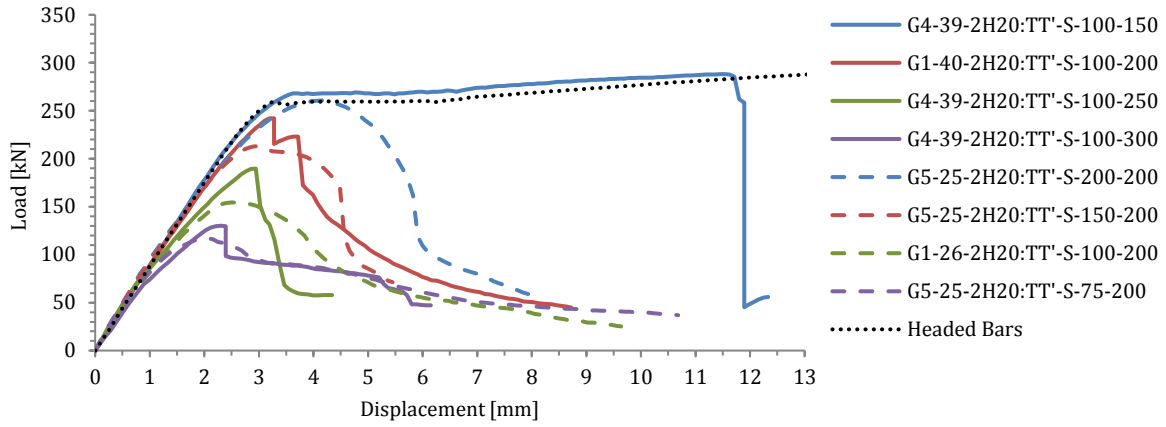

Figure 21: Test groups 4 and 5 load-displacement

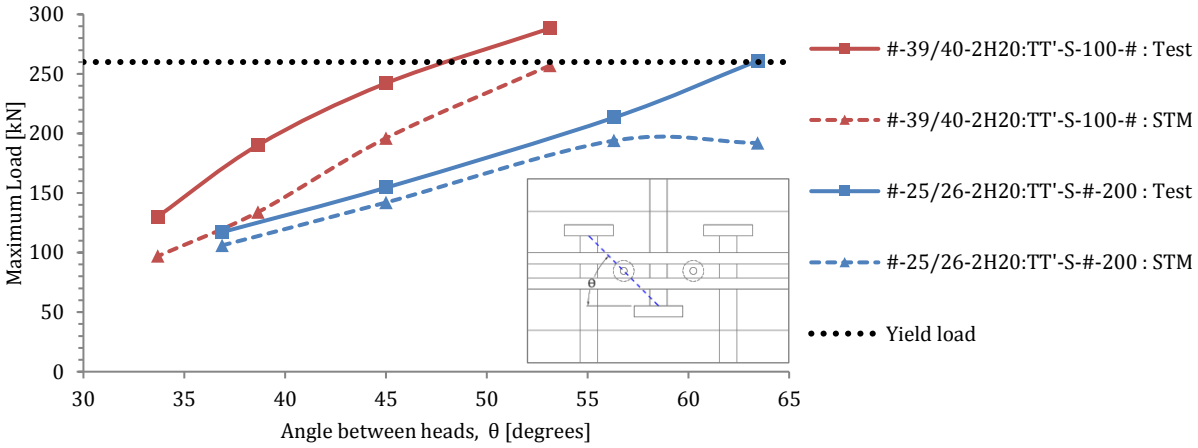

Figure 22: Effect of angle between heads

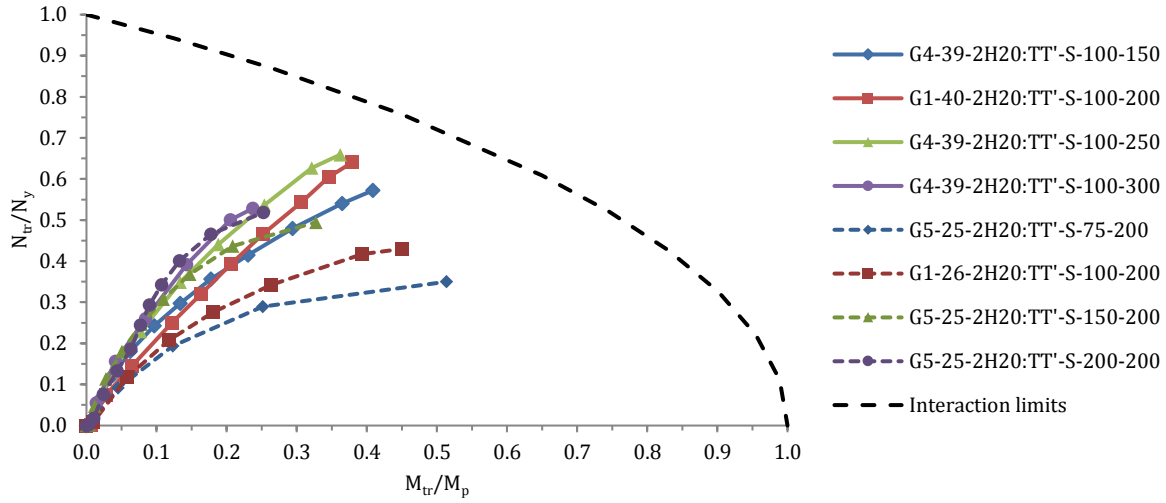

Figure 23: Test groups 4 and 5 transverse bar force interaction at S2-S3

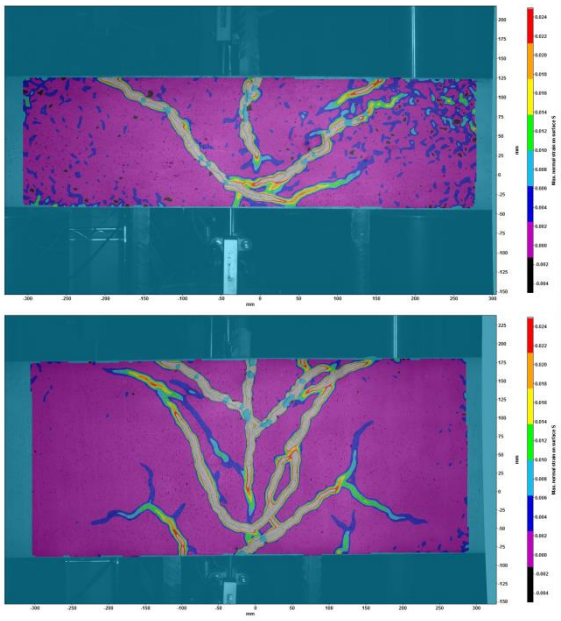

Figure 24: DIC processed images showing surface principal strains at failure: test G4-39-2H20:TT'-S-100-300 (top) and test G5-25-2H20:TT'-S-200-200 (bottom)

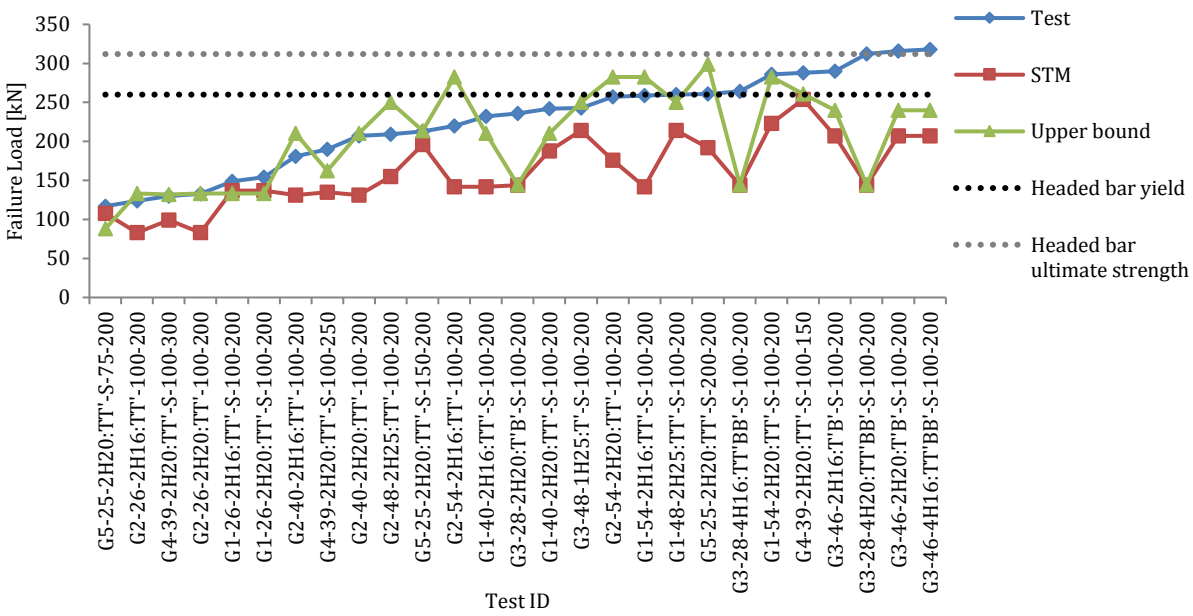

Figure 25: Comparison between test results and unfactored STM and upper bound predictions

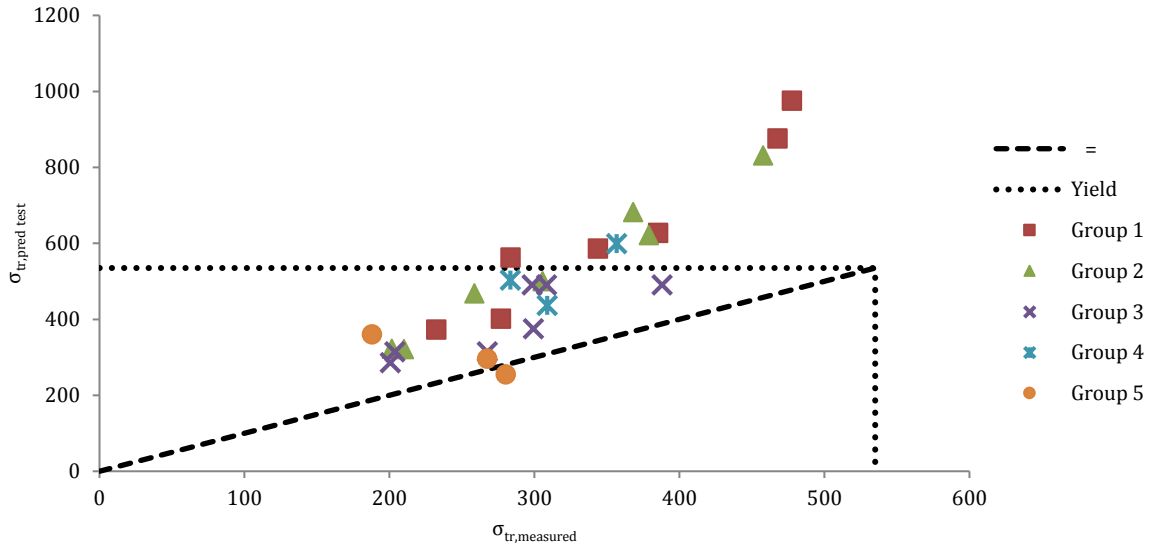

Figure 26: Predicted against measured axial stress in transverse bar

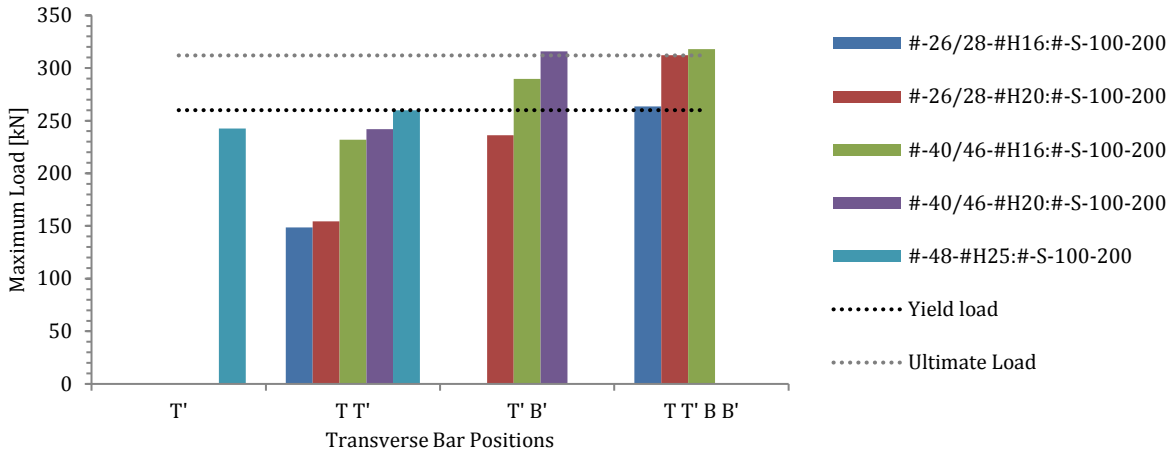

Figure 27: Effect of transverse bar arrangement

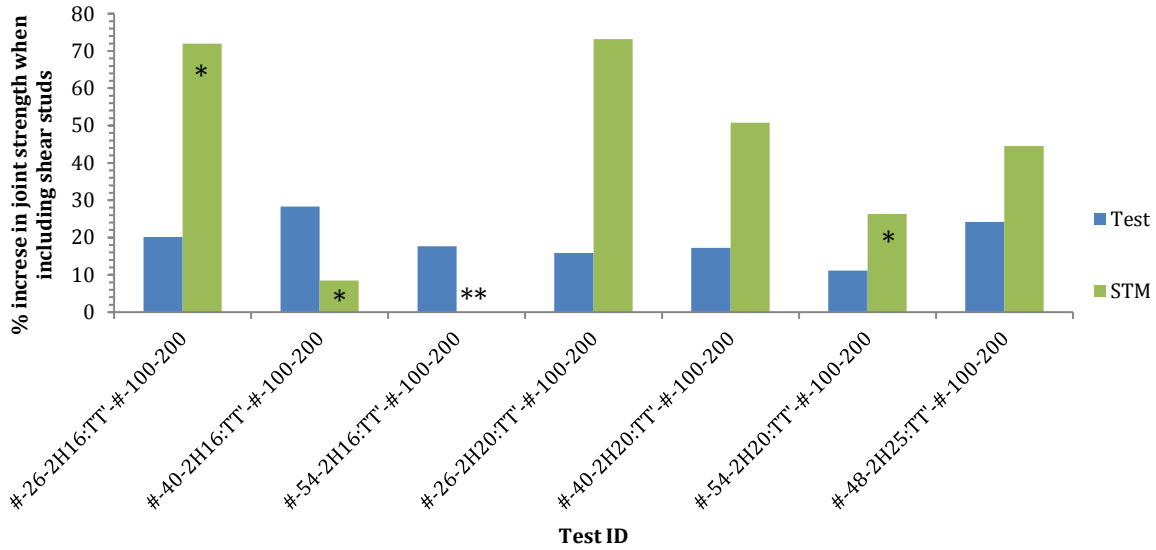

* STM failure mode of specimen with shear studs is transverse bar yield

** STM failure mode of both specimens is transverse bar yield

Figure 28: Effect of shear studs on joint strength

List of Tables

Test ID	$f_{c,cyl}$ *(MPa)*	f_{ct} *(MPa)*	$\emptyset_{tr}$ *(mm)*	Transverse Bar Positions	S_{hb} *(mm)*	L_{hb} *(mm)*	P_{test} *(kN)* {failure mode}	P_{STM} *(kN)* {failure mode}	$\frac{P_{STM}}{P_{test}}$	P_{UB} *(kN)* {failure mode}	$\frac{P_{UB}}{P_{test}}$
G1-26-2H16:TT'-S-100-200	25.6	2.38	16	T T'	200	100	149 {J}	137 {S}	0.92	133 {J}	0.89
G1-40-2H16:TT'-S-100-200	40.4	3.60	16	T T'	200	100	232 {J}	142 {T}	0.61	210 {J}	0.91
G1-54-2H16:TT'-S-100-200	54.3	4.57	16	T T'	200	100	259 {J}	142 {T}	0.55	283 {H}	1.09
G1-26-2H20:TT'-S-100-200	25.6	2.38	20	T T'	200	100	154 {J}	137 {S}	0.89	133 {J}	0.87
G1-40-2H20:TT'-S-100-200	40.4	3.60	20	T T'	200	100	242 {J}	188 {S}	0.78	210 {J}	0.87
G1-54-2H20:TT'-S-100-200	54.3	4.57	20	T T'	200	100	286 {H}	223 {T}	0.78	283 {H}	0.99
G1-48-2H25:TT'-S-100-200	48.0	4.04	25	T T'	200	100	260 {J}	214 {S}	0.82	250 {J}	0.96
G2-26-2H16:TT'-100-200	25.6	2.38	16	T T'	200	100	124 {J}	83 {S}	0.67	133 {J}	1.08
G2-40-2H16:TT'-100-200	40.4	3.60	16	T T'	200	100	181 {J}	131 {S}	0.72	210 {J}	1.16
G2-54-2H16:TT'-100-200	54.3	4.57	16	T T'	200	100	220 {J}	142 {T}	0.65	283 {H}	1.29
G2-26-2H20:TT'-100-200	25.6	2.38	20	T T'	200	100	133 {J}	83 {S}	0.62	133 {J}	1.00
G2-40-2H20:TT'-100-200	40.4	3.60	20	T T'	200	100	207 {J}	131 {S}	0.63	210 {J}	1.02
G2-54-2H20:TT'-100-200	54.3	4.57	20	T T'	200	100	257 {J}	176 {S}	0.68	283 {H}	1.10
G2-48-2H25:TT'-100-200	48.0	4.04	25	T T'	200	100	209 {J}	155 {S}	0.74	250 {J}	1.20
G3-28-2H20:T'B'-S-100-200	27.7	2.65	20	T' B'	200	100	236 {J}	144 {S}	0.61	144 {J}	0.61
G3-28-4H16:TT'BB'-S-100-200	27.7	2.65	16	T T' B B'	200	100	264 {H}	144 {S}	0.55	144 {J}	0.55
G3-28-4H20:TT'BB'-S-100-200	27.7	2.65	20	T T' B B'	200	100	312 {H}	144 {S}	0.46	144 {J}	0.55
G3-46-2H20:T'B'-S-100-200	46.1	3.80	20	T' B'	200	100	316 {H}	207 {S}	0.66	240 {J}	0.92
G3-46-4H16:TT'BB'-S-100-200	46.1	3.80	16	T T' B B'	200	100	318 {H}	207 {S}	0.65	240 {J}	0.92
G3-46-2H16:T'B'-S-100-200	46.1	3.80	16	T' B'	200	100	290 {H}	207 {S}	0.71	240 {J}	0.92
G3-48-1H25:T'-S-100-200	48.0	4.04	25	T'	200	100	243 {J}	214 {S}	0.88	250 {J}	1.03
G4-39-2H20:TT'-S-100-150	39.2	3.36	20	T T'	150	100	288 {H}	254 {S}	0.88	261 {H}	0.91
G4-39-2H20:TT'-S-100-250	39.2	3.36	20	T T'	250	100	190 {J}	135 {S}	0.71	162 {J}	0.85
G4-39-2H20:TT'-S-100-300	39.2	3.36	20	T T'	300	100	130 {J}	99 {S}	0.76	132 {J}	1.01
G5-25-2H20:TT'-S-75-200	24.8	2.13	20	T T'	200	75	117 {J}	108 {S}	0.92	88 {J}	0.75
G5-25-2H20:TT'-S-150-200	24.8	2.13	20	T T'	200	150	213 {J}	196 {S}	0.92	213 {J}	1.00
G5-25-2H20:TT'-S-200-200	24.8	2.13	20	T T'	200	200	261 {J}	192 {S}	0.74	299 {H}	1.15

Failure modes: {J} = Joint failure; {H} = Headed bar yield; {T} = Transverse bar yield; {S} = Concrete strut failure

Table 1: Test specimen details

Type	$\emptyset_b$ *(mm)*	Head size *(mm)*	f_y *(MPa)*	f_u *(MPa)*	E_s *(GPa)*
Headed bar	25	70 x 70 x 16	530	636	197
Transverse bar	25	-	552	669	185
Transverse bar	20	-	539	644	211
Transverse bar	16	-	536	640	206
Shear stud	10	Ø30	553	647	213

Table 2: Reinforcement material properties